

**Effects of Deformation on the Compressibility and Permeability of
Carrara Marble**

by Janet Chen

B.S. in Earth, Atmospheric, and Planetary Sciences
Massachusetts Institute of Technology
(1994)

Submitted to the Department of Earth, Atmospheric, and Planetary Sciences
in partial fulfillment of the requirements for the Degree of

Master of Science
at the
Massachusetts Institute of Technology
May 1995

© 1995 Massachusetts Institute of Technology
All rights reserved

Signature of author.....
Department of Earth, Atmospheric, and Planetary Sciences
May, 1995

Certified by.....
Professor Brian Evans
Thesis Supervisor

Accepted by.....
Thomas H. Jordan
Department Chairman

Lindgren
WITHDRAWN
MASSACHUSETTS INSTITUTE
OF TECHNOLOGY
FROM
JUN 05 1995
MIT LIBRARIES
LIBRARIES

Effects of Deformation on the Compressibility and Permeability of Carrara Marble

**by
Janet Chen**

Submitted to the Department of Earth, Atmospheric, and Planetary Sciences on May 26, 1995 in partial fulfillment of the requirements for the degree of Master of Science

Abstract

Microcracking resulting from axial compression was examined by observing post-deformation compressibility and permeability in experiments on Carrara marble. Samples were deformed at room temperature to axial strains of 3% and 5% at confining pressures between 80 MPa and 250 MPa. Volumetric compressibilities after axial unloading increased with strain. Samples deformed under low confining pressure had large changes in compressibility. Isotropy increased with high confining pressure and strain.

Permeability after axial unloading was tested at effective pressures between 2-170 MPa at constant temperature of 47°C. Permeability increases with high strain and low effective pressure. At low effective pressure of 30 MPa, the two factors offset each other so that the sample deformed to 3% axial strain at 100 MPa was as permeable as the one that endured 5% at 190 MPa.

Acknowledgements

I am greatly appreciative of Brian Evans for his insights, guidance, and humor. I thank him for giving me the opportunity to work on rock mechanics research because I have learned and enjoyed much from working in his laboratory.

Gunter Siddiqi generously committed time and energy in training me in the laboratory. Discussions with him throughout the duration of the project were essential. I am indebted to him for all he has unselfishly taught me.

Steve Karner and my officemates, Gretchen Eckhardt and Lynn Smith all have been supportive and helpful to me. I am grateful because each of them made my work easier.

During my 5 years at MIT, I have been fortunate enough to have the friendship of Jung Yu. I thank him for the fun companionship we have.

I treasure my family members for their constant loving support.

Table of Contents

1 Introduction.....	6
2 Experimental Procedures.....	8
2.1 Stiff Press Experiments.....	8
2.1.1 Sample Preparations for Triaxial Deformation Experiments.....	8
2.1.2 Pressure-volume and Axial Deformation Testing.....	9
2.2 Permeameter Experiments.....	10
2.2.1 Sample Preparations for Permeability Experiments.....	11
2.2.2 Permeability Testing.....	11
3 Results.....	13
3.1 Axial Compression.....	13
3.2 Compressibilities Before and After Axial Deformation.....	14
3.3 Permeabilities.....	15
4 Discussion.....	17
4.1 Stiffness and Strength During Axial Deformation.....	17
4.2 Volumetric Strain During Axial Deformation.....	18
4.3 Compressibility.....	18
4.4 Permeability.....	19

5 Conclusions.....21

Figures.....23

Tables.....44

References.....46

Chapter 1: Introduction

Below pressures and temperatures necessary for fully plastic deformation, cataclastic flow is a major strain accommodating deformation mechanism. In some past studies [*Fredrich et al., 1989; Hirth and Tullis, 1994*], data taken during deformation have been used in conjunction with microstructural imaging to examine the transitions in both localization and deformation mechanisms. Between confining pressures of 30-300 MPa, microcracking, twinning, and dislocation gliding all occur. Dislocation gliding occurs at confining pressures as low as 50 MPa. Anisotropy decreases at high confining pressures [*Fredrich et al., 1989*]. Active dislocations are responsible for the transition from cataclastic faulting to semibrittle faulting. The change from localized to distributed deformation characterizes the transition from semibrittle faulting to semibrittle flow. The transition from semibrittle flow to dislocation creep is probably caused by more mobile grain boundaries at high temperatures [*Hirth and Tullis, 1994*]. A major goal is to understand how permeability is related to deformation. Permeabilities and changes in apparent porosity are higher during deformation at low confining pressure [*Zhang et al., 1994*]. This study focuses on the effects of deformation on compressibility and permeability.

Cataclastic flow causes microcracking. Theoretically, this cracking will increase the compressibility [*Walsh, 1965a*]. Cracking during axial compression in Westerly granite is predominantly in the axial direction [*Brace et al., 1966*]. The relative effects of confining pressure and strain of microcracking on compressibility need to be investigated.

Cracked samples are more permeable. Presumably, permeability measured in the axial direction increases after compression because cracking occurs predominantly parallel to the axis of compression. As previously stated, *Zhang et al. [1994]* have found that samples deformed under low confining pressure are more permeable than higher ones. This study examines permeabilities through a range of effective pressures after deformation has ended.

Chapter 2: Experimental Procedures

Two types of experiments were conducted on Carrara marble for this study. Triaxial deformation experiments and permeability tests were not performed on the same machine. This chapter presents the general operations, sample preparations, and testing procedures for the stiff press and the permeameter.

2.1:Stiff Press Experiments

Standard triaxial deformation experiments were conducted on a stiff deformation apparatus shown schematically in Figure 1. Confining pressure up to 100 MPa was generated from pressurized argon gas using a gas pump and was monitored with a Heise gauge. An oil-driven intensifier was used to reach higher confining pressures. A piston driven by a ball-screw mechanism provided the axial load, measured by a load cell. For this study, axial strain rate was kept constant at $10e-5$ /second. Precision electric resistance strain gauges were used to determine axial and radial strain. Strain gauges and A/D converter were similar to those used in *Fredrich et al. [1989]* where strain uncertainty was 0.01%.

2.1.1:Sample Preparations for Triaxial Deformation Experiments

Deformation samples were one inch long and one-half inch in diameter. Since water influences mechanical behavior, sample preparations minimized water content. Prior to testing, we dried the samples in vacuum at room temperature for at least ten hours.

Each sample was jacketed in a copper foil cover 4.15mm by 2.45mm and two copper end caps. The cover was tightly wrapped around the samples and lead soldered together. The two end caps of 13.50 mm diameter were then similarly soldered. Once jacketed, the sample was pressurized to 100 MPa to collapse the jacket tightly onto the sample.

As samples were aligned with the piston providing the axial load, the principal stress axes were assumed to be parallel and perpendicular to the sample length axis. A strain gauge was mounted on the jacket in each of these directions. They were mounted with a bond adhesive of methy-2-cyanoacrylate after the jacket had been treated with 400 grit silicon carbide grinding paper, acid conditioner, and alkaline neutralizer. Since strains in this study were small, volumetric strain was determined from equation 1.

$$\text{volumetric strain} = \text{axial strain} + 2 * \text{radial strain} \quad (1)$$

2.1.2: Pressure-volume and Axial Deformation Testing

Experiments began with the pressure-volume compressibility test. The samples were then axially deformed past the yield point to various degrees of permanent strain. Afterwards, a post-deformation compressibility test was conducted to determine the effects of deformation.

In the axial compression experiments, first, argon gas created the confining pressure. We were interested in exploring semibrittle deformation so confining pressures ranging from 80 - 250 MPa were chosen. At these pressures Carrara marble axially deforms to at least 3% strain without fracturing [Fredrich et al., 1989]. For this study,

most of the samples were deformed to 3% axial strain, well within the 6% limit of the strain gauges. At the start, the piston was positioned just above the hit point. As it compressed the sample at the axial strain rate of $10e-5$ /second, recordings of load, strains, and piston position were made every 2 seconds.

2.2: Permeameter Experiments

The permeameter was designed for the transient flow method of determining permeability [Bernabe, 1987]. Presumably, flow obeyed Darcy's law (equation 2).

$$\text{Volumetric flow rate (m}^3\text{/s)} = -(k/\mu) (dp/dx), \text{ where} \quad (2)$$

k = permeability (m^2),
 μ = fluid viscosity (Pa-s), and
 dp/dx = applied pressure gradient (Pa).

Permeabilities were determined from the decay of pressure when fluid flowed through the sample. Decay time was inversely proportional to permeability according to equation 3 [Bernabe, 1987].

$$\text{Pressure decay (Pa)} \approx \exp[-((A*k*(C_u+C_d)) / (\mu*L*C_u*C_d))*t] \text{ where} \quad (3)$$

A = sample cross sectional area (m^2),
 k = permeability (m^2),
 μ = fluid viscosity (Pa-s),
 L = sample length (m),
 t = time (s), and
 C_d and C_u = compressive storages of upstream and downstream reservoirs ($\text{m}^3\text{/Pa}$).

The permeameter, shown schematically in Figure 2, allowed for control of confining pressure, pore fluid pressure, and the pressure pulse sent from the upstream to

the downstream reservoir. Pressurized kerosene from an air-driven fluid pump created confining pressure, and pore fluid pressure was obtained by hand-pumping distilled water. Heise gauges monitored both pressures. A thermometer in the isothermal airflow oven chamber was used to make sure temperature stayed at $47\pm 1^\circ\text{C}$. Temperature had to be controlled because it could have perturbed the pressure pulse decay. Increasing the upstream reservoir volume through a metering valve generated the pressure pulse. An absolute pressure transducer and a differential pressure transducer measured the pressure differential between reservoirs. The permeameter is described in more detail by *Bernabe [1987]*.

2.2.1: Sample Preparations for Permeability Experiments

Permeability experiments followed axial deformation. To remove the copper jacketing from stiff press testing, each end cap was sawed off, and the copper foiled was peeled away. Dejacketing made samples about 3-4 mm shorter than their original lengths.

Prior to permeability testing, the samples were saturated by immersion in distilled water for several hours while under vacuum. They were then jacketed in heat-shrink tubing and Tygon rubber tubing.

2.2.2: Permeability Testing

Permeability was measured at a range of effective pressures for each sample. To obtain different effective pressures, confining pressure was raised while pore fluid pressure was kept constant at a value below 200 MPa. After the system reached the desired effective pressure, it was left to equilibrate for at least half an hour. Then, the pressure in

the upstream reservoir was raised by about 1 MPa, and the subsequent pressure decay was monitored for periods ranging from minutes to hours depending on the decay rate. Pressure transducer readings were made at frequencies ranging from 0.2 Hz to 9 Hz.

Chapter 3: Results

The purpose of this study is to examine the effects of axial compression on compressibility and permeability. In this chapter, the axial deformation is examined closely before its effects on compressibility and permeability are shown.

3.1: Axial Compression

The differential stress-axial strain relation of Carrara marble is shown in Figure 3. To reduce noise, each point plotted in all of the stiff press experiment figures represents the average differential stress and axial strain for an eight second interval.

The deformation curve run at 100 MPa confining pressure loops several times. This sample was reloaded three times along the way to 3% axial strain to verify that unloading and reloading the sample had minimal effect on the stress-strain behavior. Figure 4 shows the 100 MPa curve in isolation. In every case, the reloading curve rejoins the original curve with minimal offset.

At confining pressures between 80-250 MPa, the samples' stress-strain behavior evolves with increased differential stress in a similar pattern. Up to a level of axial strain of about 0.5%, Carrara marble is relatively stiff. Then, as differential stress continues to increase, it softens as yielding with permanent strain occurs. The softening stabilizes by about 1% axial strain when the Carrara marble shows nearly linear stress-strain behavior.

Confining pressure has two clear effects on the mechanical behavior during axial compression. First, larger differential stress is required for yielding at greater confining pressures. For confining pressure of 80 MPa, steady state has been reached by differential

stress of 175 MPa. At 250 MPa confining pressure, 300 MPa of differential stress is required to display nearly linear stress-strain behavior.

The other effect of confining pressure is on the final hardening rate. From Figure 3, the final slopes of each curve are steeper for the higher confining pressure. Table 1 shows the slope and linear correlation coefficient of each curve in the range from 2-3% axial strain.

The relation between volumetric strain and axial strain is presented in Figure 5. For every confining pressure used in this study, the relation between volumetric strain and axial strain becomes nearly linear. There is a clear trend that the slopes become more negative at lower confining pressures. At 250 MPa, the sample contracts, but the sample at 80 MPa expands.

3.2: Compressibilities Before and After Axial Deformation

To study the effects of axial compression on volumetric compressibility, the compressibility of undeformed Carrara marble should be carefully observed. Figure 6 shows the pressure-volumetric strain relation of three undeformed Carrara marble samples. In Figure 6 and all of the compressibility figures, each data point shows averaged values taken at each confining pressure. For each sample, there is a similar shape to the curves. The samples begin with relatively low stiffness. Then, they stiffen as confining pressure rises. By about 40 MPa, pressure and volumetric strain are nearly linearly related. Table 2 shows the slopes beyond 40 MPa for each curve in Figures 6-10.

Comparisons of the pressure-volumetric strain relations for Carrara marble before and after axial deformation are shown in Figures 7-9. Figure 10 is a compilation of the post-deformation compressibilities for the samples that were deformed to 3% axial strain. There is less variability in compressibility after deformation. Table 2 indicates that when samples are taken to the same axial strain, compressibility changes are related to confining pressure during deformation. Lower confining pressures results in larger changes in slope.

The linear compressibilities, which refer to the relations between pressure and axial and radial strains, are shown in Figures 11-13 for Carrara marble before and after axial deformation to 3%. All undeformed samples behave similarly in the axial and radial directions. After deformation, the difference between the axial and radial curves becomes more severe at lower confining pressures.

A comparison was made between 3% and 5% axial strain deformation. Figure 14 shows the compressibility behavior before and after the two levels of deformation at the same confining pressure of 190 MPa. Table 2 shows that the change in slope for the sample deformed to 5% at 190 MPa is greater than for any of the samples deformed to 3%. Figure 15 shows the linear compressibilities of this sample. The slope changes in this figure are similar for the axial and radial directions. Table 3 compares the linear compressibilities for the samples compressed to 3% and 5% at 190 MPa.

3.3: Permeabilities

All deformed samples are more permeable than the undeformed samples. Figure 16 illustrates changes of permeability with effective pressure for different strains and

confining pressures. The undeformed sample is the least permeable. In all cases, permeability decreases with increasing effective pressure.

Chapter 4: Discussion

During semibrittle deformation of Carrara marble, strength, volumetric strain, and linear compressibility all depend on confining pressure. High confining pressure allows samples to support greater differential stress. It also apparently leads to isotropic deformation. Low confining pressure during axial compression enhances dilatancy. Deformed samples are more permeable than undeformed samples, and effective pressure hinders permeability.

4.1: Stiffness and Strength During Axial Deformation

The softening effect and strength-dependence on confining pressure have been seen in many studies of Carrara marble [Edmond and Paterson, 1972; Fredrich *et al.*, 1989; Fisher and Paterson, 1989; Zhang *et al.*, 1994]. Figure 17 and 18 compare axial deformation from this study to that of previous studies. From Figure 17, the Carrara marble of this study behaves within the range of the other two samples although it was not tested on the same machine as other two. It is weaker than Zhang's marble, while it is stronger than Edmond's sample. Figure 18 compares axial compression performed on the same deformation apparatus. The results vary minimally. The small difference in strength, which is less than 50 MPa, is attributed to variation among Carrara marbles.

Microcracking from axial compression causes the softening effect. The experimental results support the theory that the presence of cracks in a solid will lower the effective Young's modulus. For a theoretical treatment of the effects of cracks on Young's modulus, see [Walsh, 1965b].

The strength or differential load that a sample endures before softening increases with confining pressure. In Figure 3, the curves begin steeply before leveling off as the sample softens. Samples under higher confining pressure reach a higher differential load before softening because the radial stress caused by the confining pressure supports the axial load by preventing cracking.

4.2: Volumetric Strain During Axial Deformation

For the samples deformed at low confining pressures around 80 MPa, there was volume expansion during deformation. This dilatancy effect occurs at low confining pressure as previously observed in Carrara marble [*e.g. Fredrich et al., 1989*] as well as granites, and it is the result of microcracking [*e.g. Brace et al., 1966*]. Results of this study agree with those previously done [*Edmond and Paterson, 1972 and Fredrich et al., 1989*] in showing that confining pressure hinders dilatancy. At high confining pressure of 250 MPa, there is contraction rather than expansion. Figures 19 and 20 compare the volumetric strain results of this study with previous studies [*Edmond and Paterson, 1972; Fredrich et al., 1989*]. The Carrara marble in this study was less dilatant than in past experiments.

4.3: Compressibility

The volumetric compressibility of rocks has been shown to decrease as cracks close at high confining pressure [*Walsh, 1965a*]. At higher pressures, cracks are mostly shut, and the compressibility would be closer to that of an uncracked sample. After axial compression, samples remain highly compressible for greater amounts of volumetric strain

before eventually stiffening. When cracking occurs, there is a larger crack volume to close before the sample will behave stiffly.

Confining pressure and the level of deformation both influence compressibility. At higher strains, more cracking occurs, and the volume of crack susceptible to closing is larger. Since cracks do not close completely, more cracking will add to the volume that can not be closed. Compressibility is less likely to return to pre-deformation values under low confining pressures.

From the linear compressibility results, high confining pressure and high strain lead to isotropic deformation. Mechanical data indicating an increase in isotropy with increased confining pressure is compatible with microstructural observations [*Fredrich et al., 1989*]. Samples become more isotropic at higher strains because at greater differential stress, rupture will eventually begin on cracks not aligned axially.

4.4 Permeability

Samples become more permeable when deformed. Permeability increases because the extension and connection of cracks enhance fluid flow. This increase is compatible with previous results [*Zhang et al., 1994*]. A comparison of permeability results for deformation at 100 MPa confining pressure is shown in Figure 21. Both studies show an increase in permeability with strain. Although the Carrara marble in this study is initially less permeable than the one used by Zhang, it is easier to crack. The slope in Figure 21 is steeper for the Carrara marble used in this study.

High strain and confining pressure offset each other in influencing permeability. In Figure 16, at low effective pressure of 30 MPa, the sample deformed to 5% axial strain at 190 MPa is as permeable as the one deformed to 3% at 100 MPa. Permeability is increased by high strain and low confining pressure. The effect of the additional 2% of strain is offset by the additional 90 MPa.

The permeability of the sample deformed at 250 MPa is suspiciously high (Figure 16). The tests show that it is the most permeable sample, but this is not compatible with the compressibility results or previous permeability tests [Zhang *et al.*, 1994]. The sample deformed at 250 MPa had the least compressibility change, and Zhang *et al.* [1994] determined that high confining pressures led to low permeabilities. The high permeability values in this study are most likely the result of ineffective jacketing. If the jacket was not wrapped around the sample tightly enough, flow between the jacket and the sample could have altered the pressure pulse decay.

Chapter 5: Conclusions

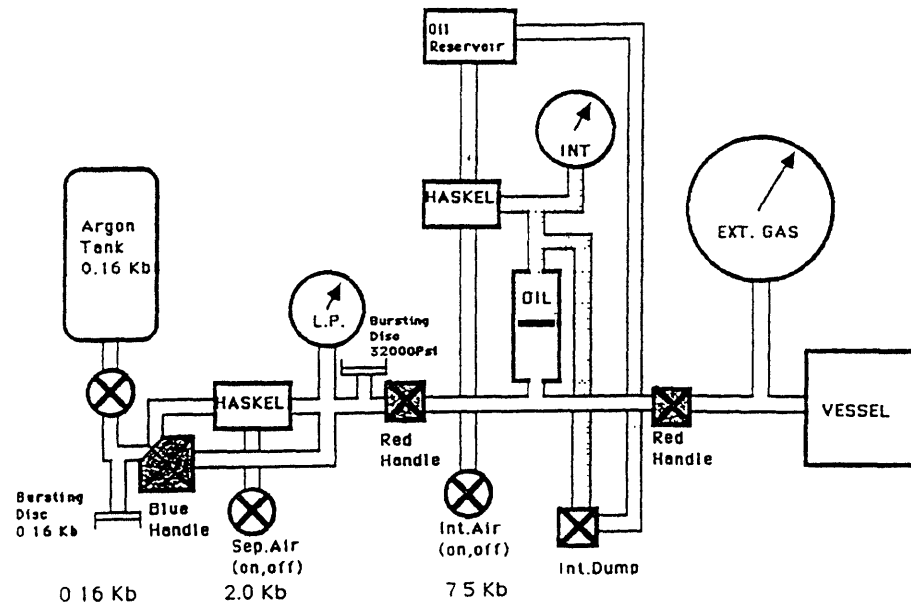
Deformation increases volumetric compressibility because cracks propagate. Low confining pressure during deformation leads to a more drastic final compressibility change. When more cracking occurs during low confining pressure compression, there is more crack volume that never completely closes during compressibility tests after deformation. Samples deform isotropically at high confining pressure or strain. Linear compressibility results show that axial and radial deformation become more alike under either of these conditions.

Carrara marble is more permeable after axial deformation as a result of connected microcracking. Strain increases permeability while effective pressure decreases it. At 30 MPa effective pressure, comparison of samples deformed to 3% and 5% axial strain shows that the two percent of additional strain is equivalent to lowering the effective pressure 90 MPa. The tradeoff between strain and effective pressure presumably does not remain constant for different strains.

The interpretations presented should be examined further. In future studies, systematic microstructural observations could be used in determining the nature of post-deformation cracks. Also, a fuller range of strains and pressures may be used so that a quantitative model of the effect of deformation on compressibility can be developed based on empirical strain and confining pressure data without relying on crack statistics. Continued testing of the effect of deformation on permeability is also required to follow the evolution of the strain-effective pressure tradeoff. This deformation study did not

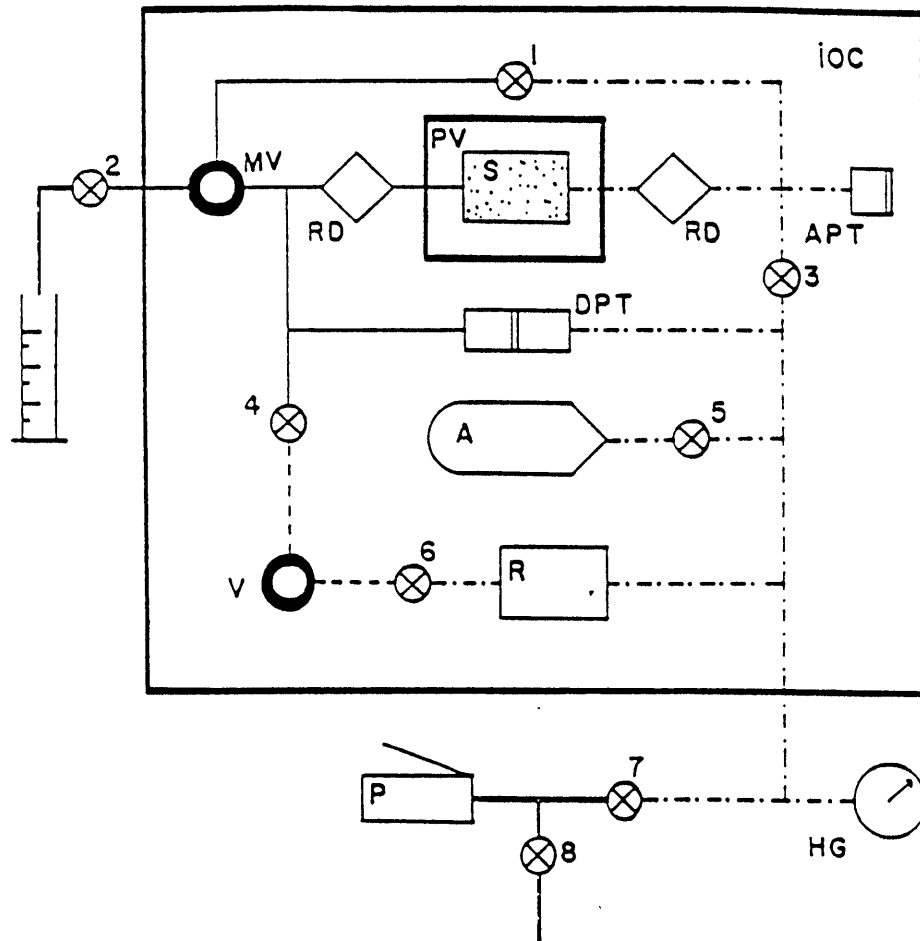
involve pore pressure. A future goal of work in this area is an understanding of the role pore fluids play during crack propagation.

Figure 1
Schematics of Stiff Press Machine



L.P. = line pressure; INT= intensifier

Figure 2
(from Bernabe, 1987)



A sketch of the apparatus. The various elements are indicated by the following abbreviations: MV - metering valve; PV - pressure vessel; S - sample; IOC - isothermal oven chamber; RD - rupture disk; APT - absolute pressure transducer; DPT - differential pressure transducer; A - accumulator; V - volumeter; R - 40cm³ reservoir; HG - Heise gage; P - pump; 1 to 8 - valves. The solid lines represent the tubings of the upstream reservoir (transient flow method), and the dotted lines those of the downstream reservoir. The reservoir drawn with dashed lines can be added to either the upstream or the downstream reservoirs in order to increase their compressive storage.

Figure 3: Stress-strain behavior during axial compression

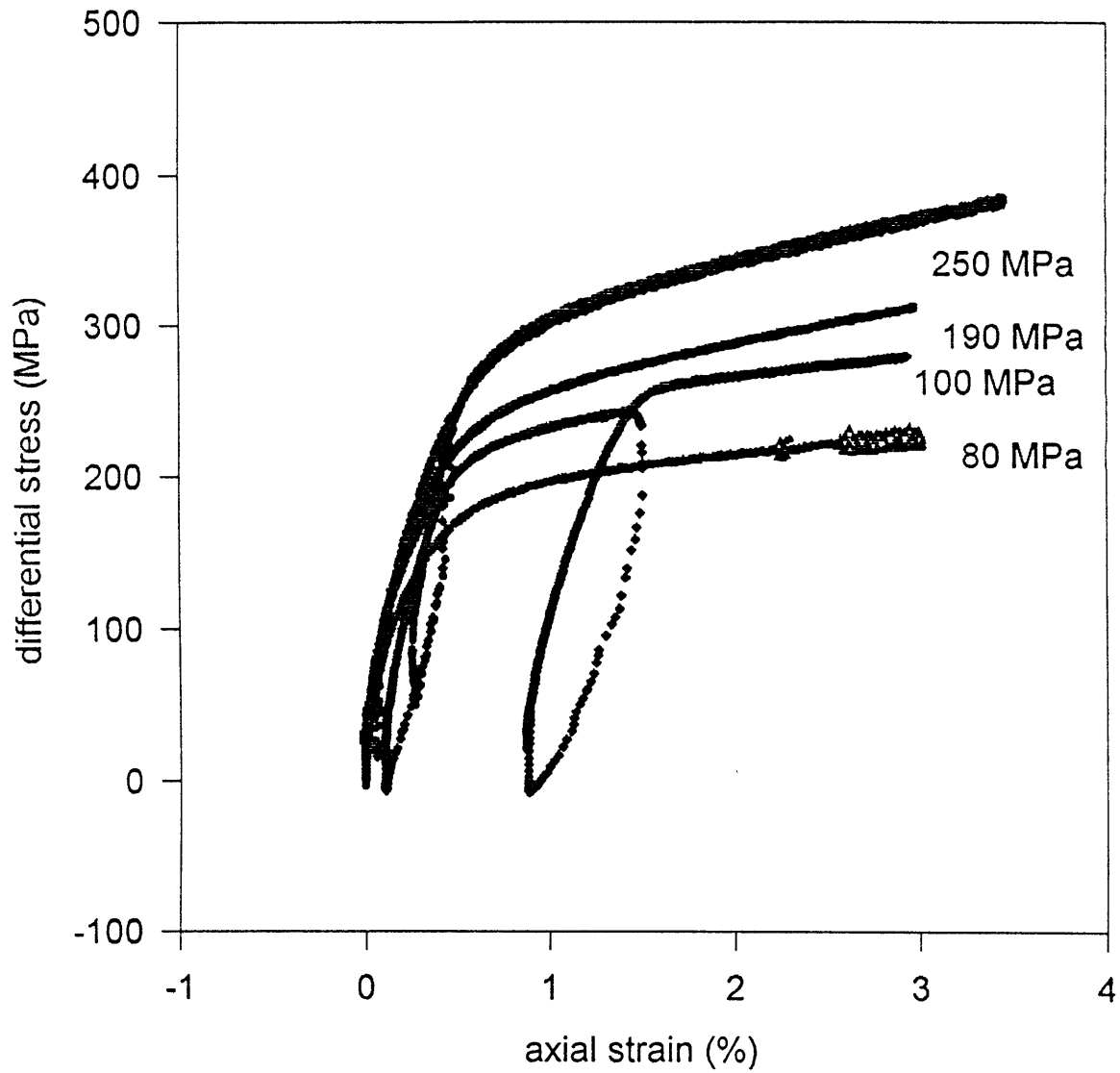


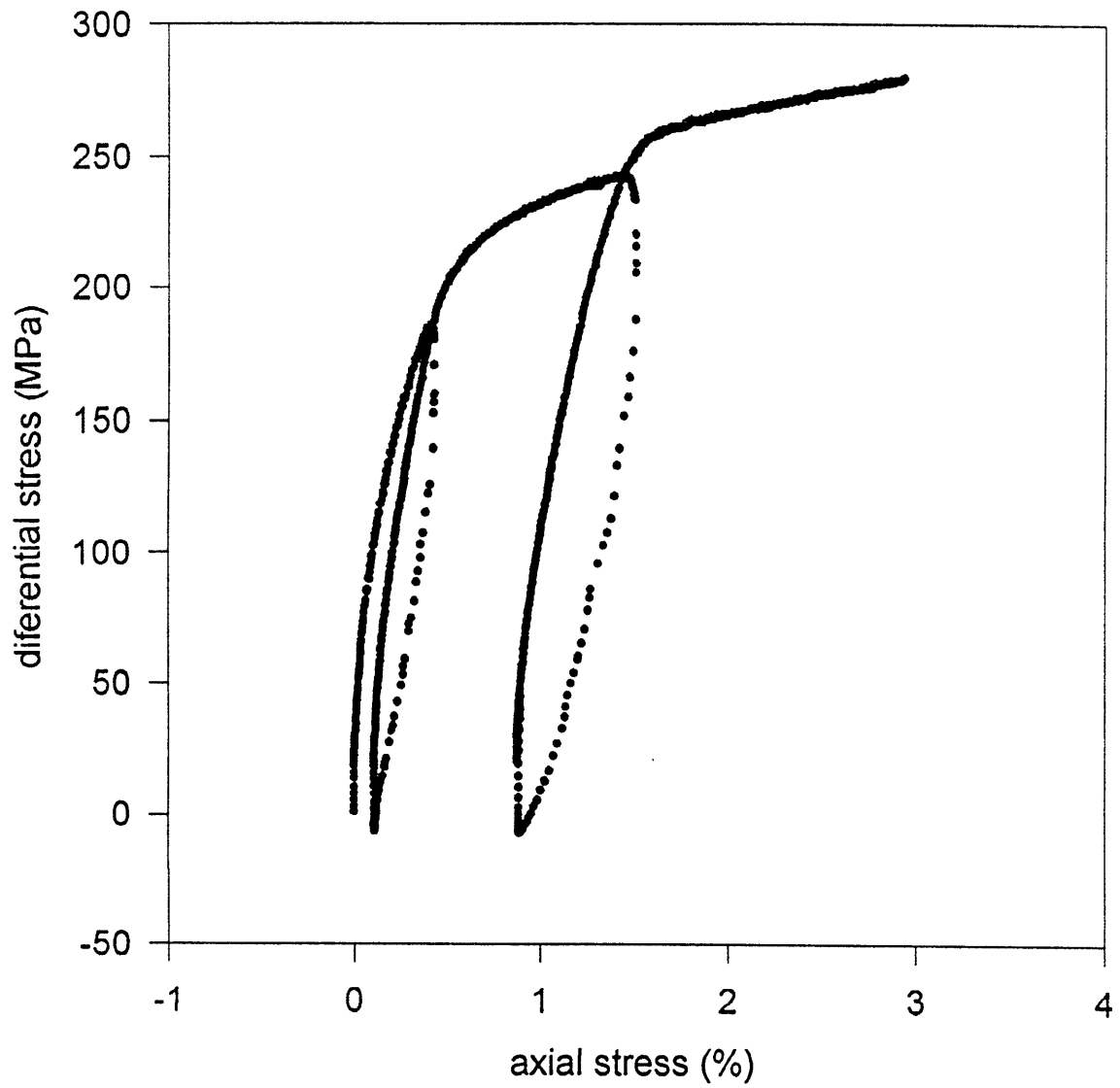
Figure 4: Axial compression at 100MPa

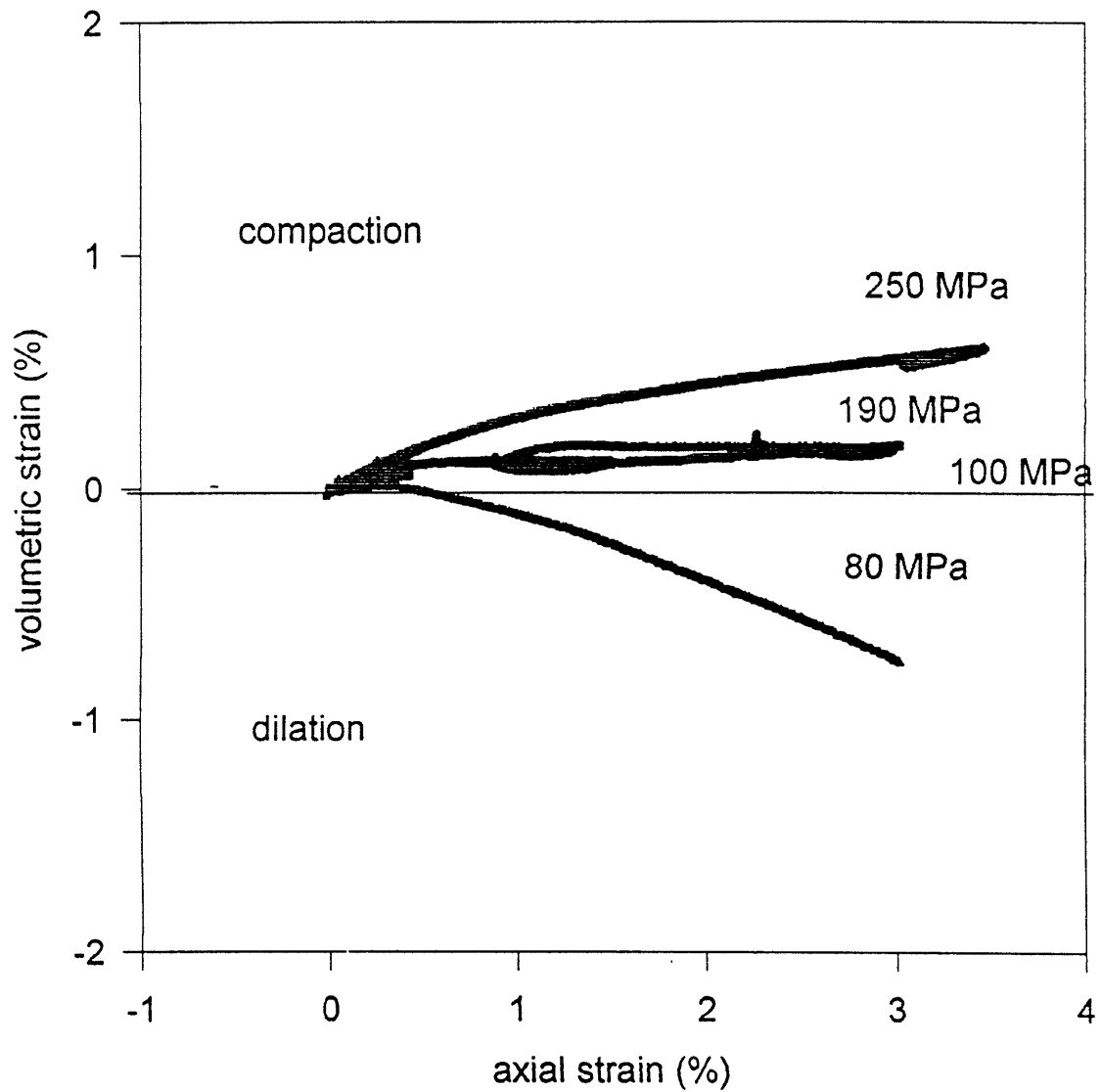
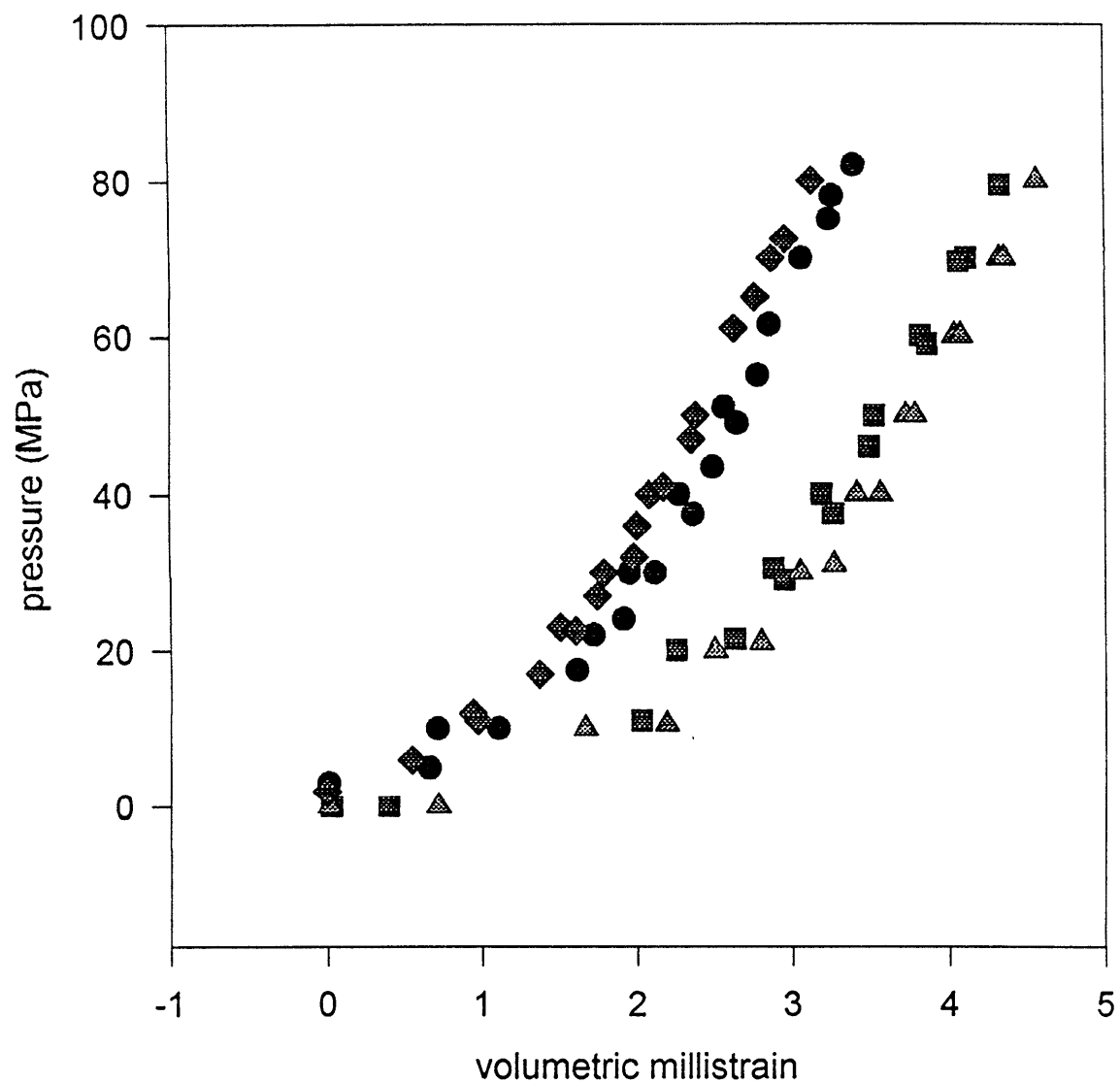
Figure 5: Volumetric-axial strain during axial compression

Figure 6: Compressibility of undeformed Carrara marble

◆ before 3% @ 250 MPa

■ before 3% @ 190 MPa

● before 3% @ 100 MPa

▲ before 3% @ 80 MPa

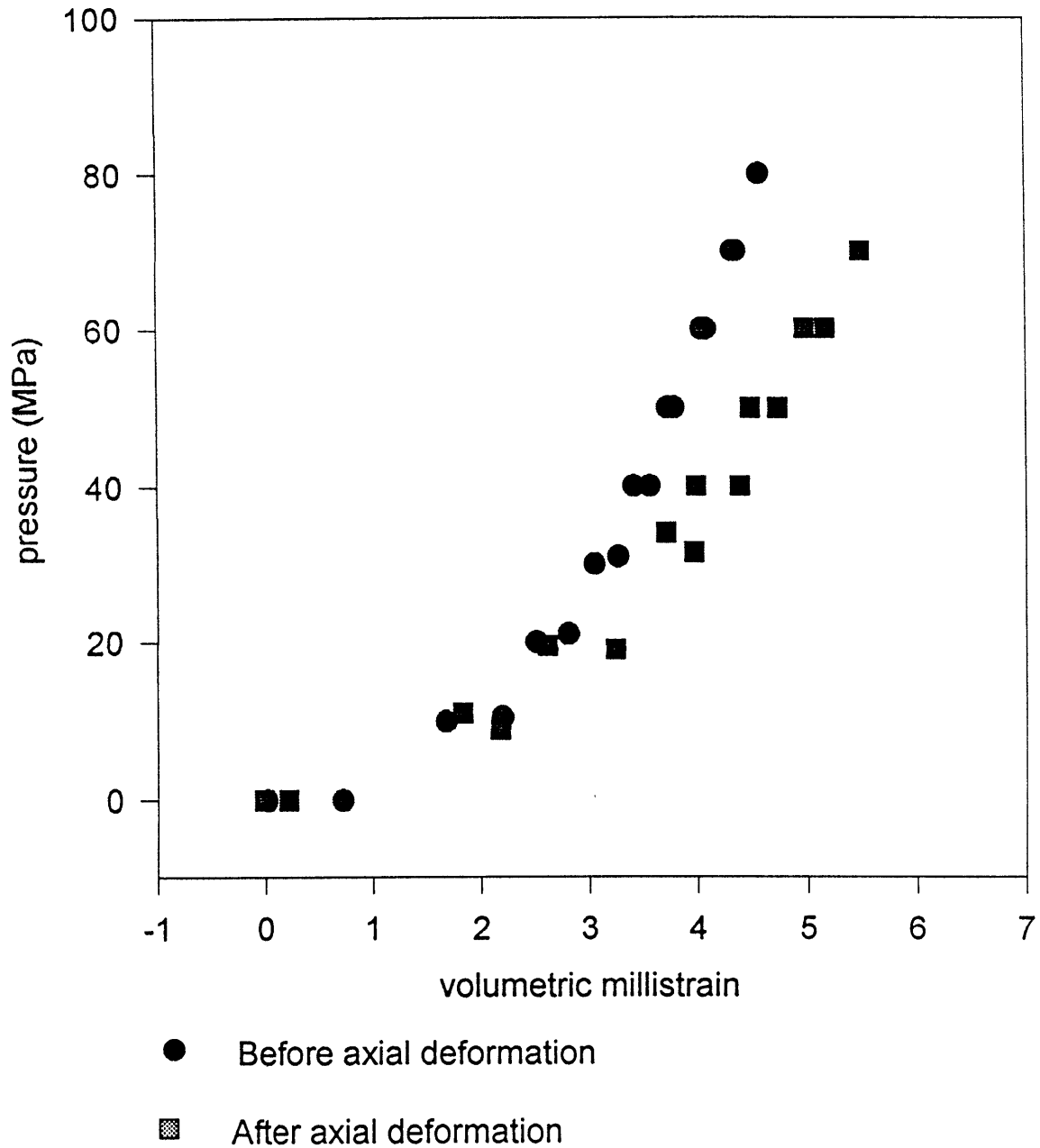
Figure 7: Compressibility (3% ax.st. @ 80MPa)

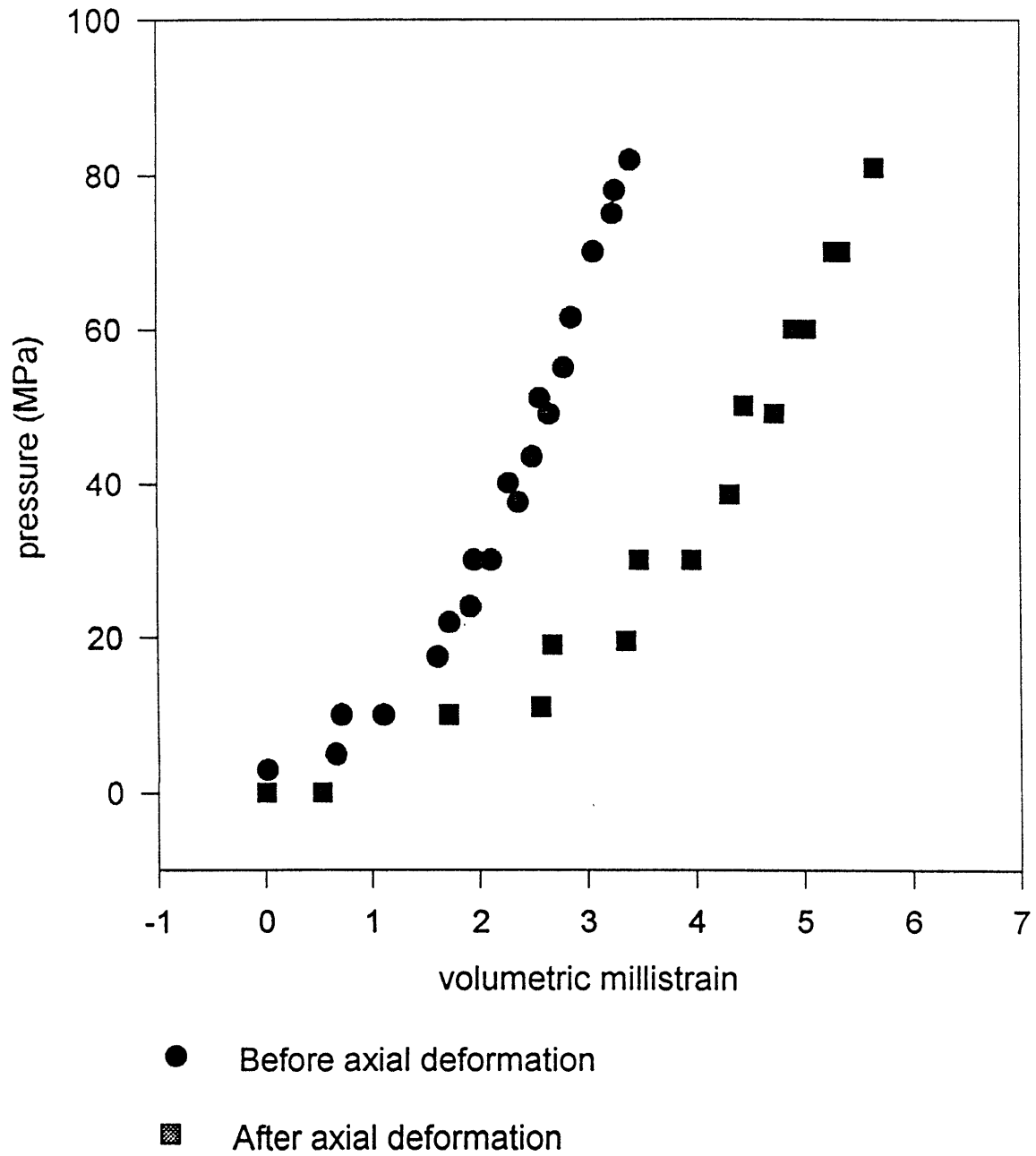
Figure 8: Compressibility (3% ax. st. @ 100MPa)

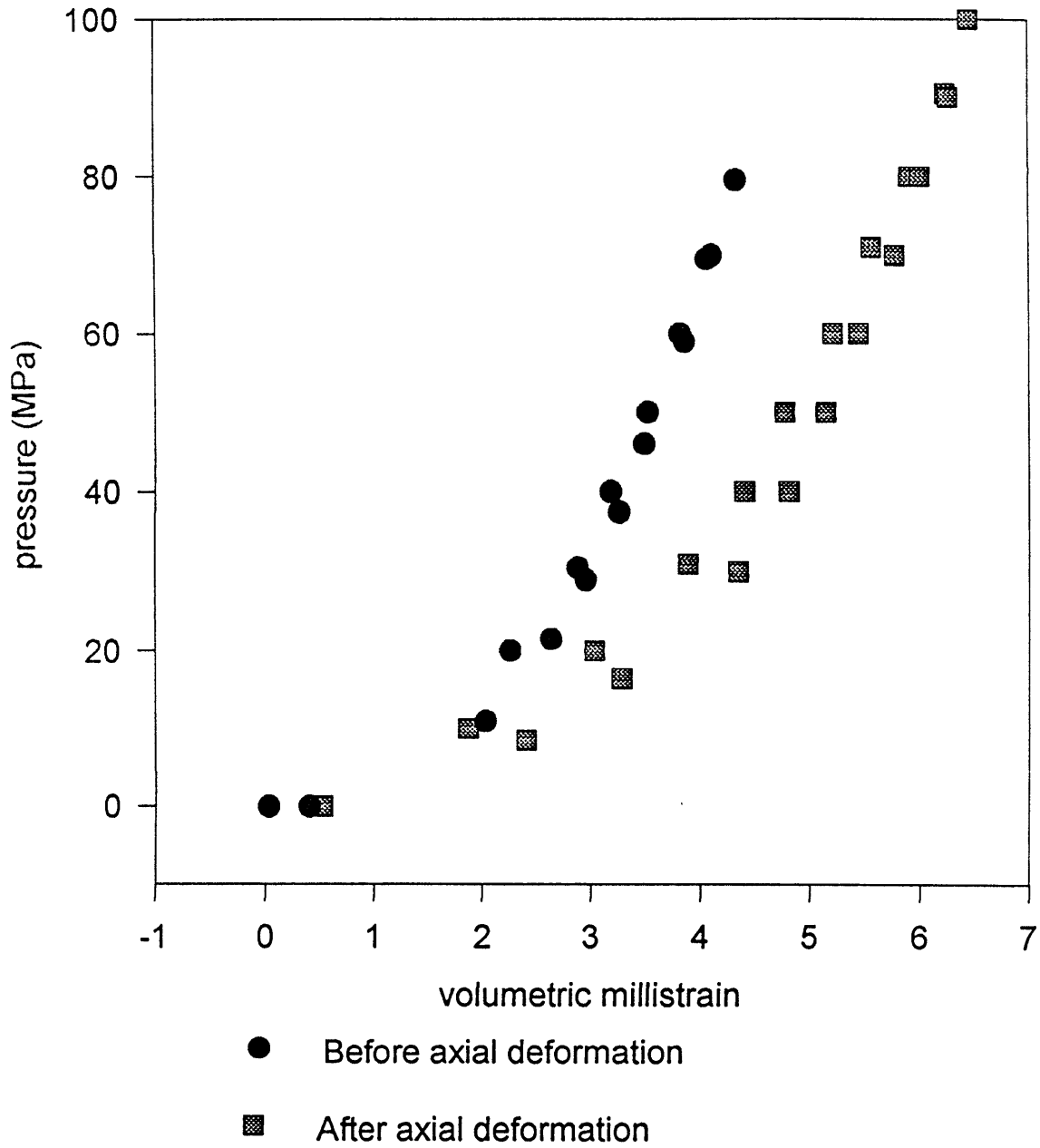
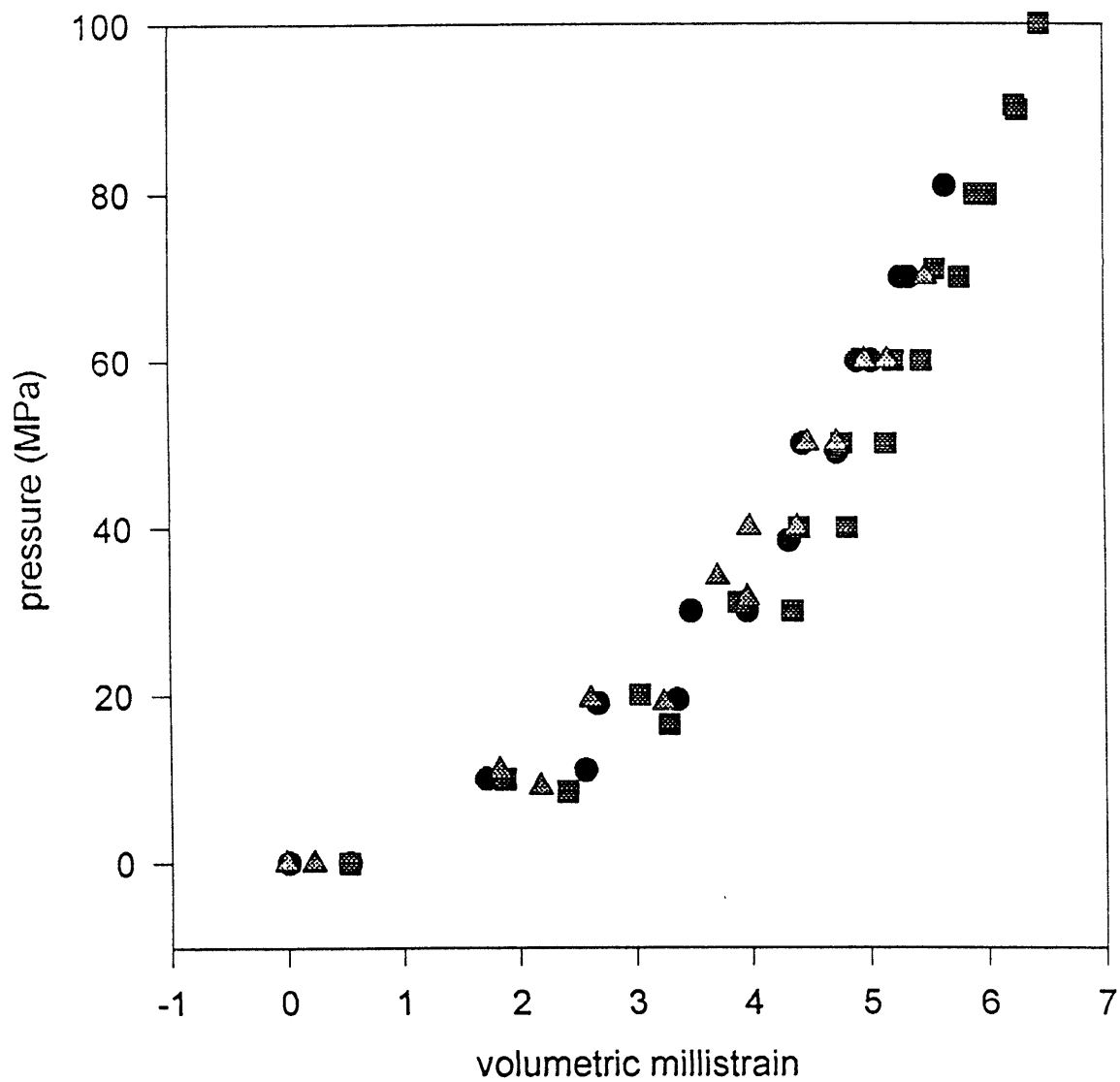
Figure 9: Compressibility (3% ax. st. @ 190MPa)

Figure 10: post-deformation compressibilities

▲ 3% axial strain @ 80 MPa

● 3% axial strain @ 100 MPa

■ 3% axial strain @ 190 MPa

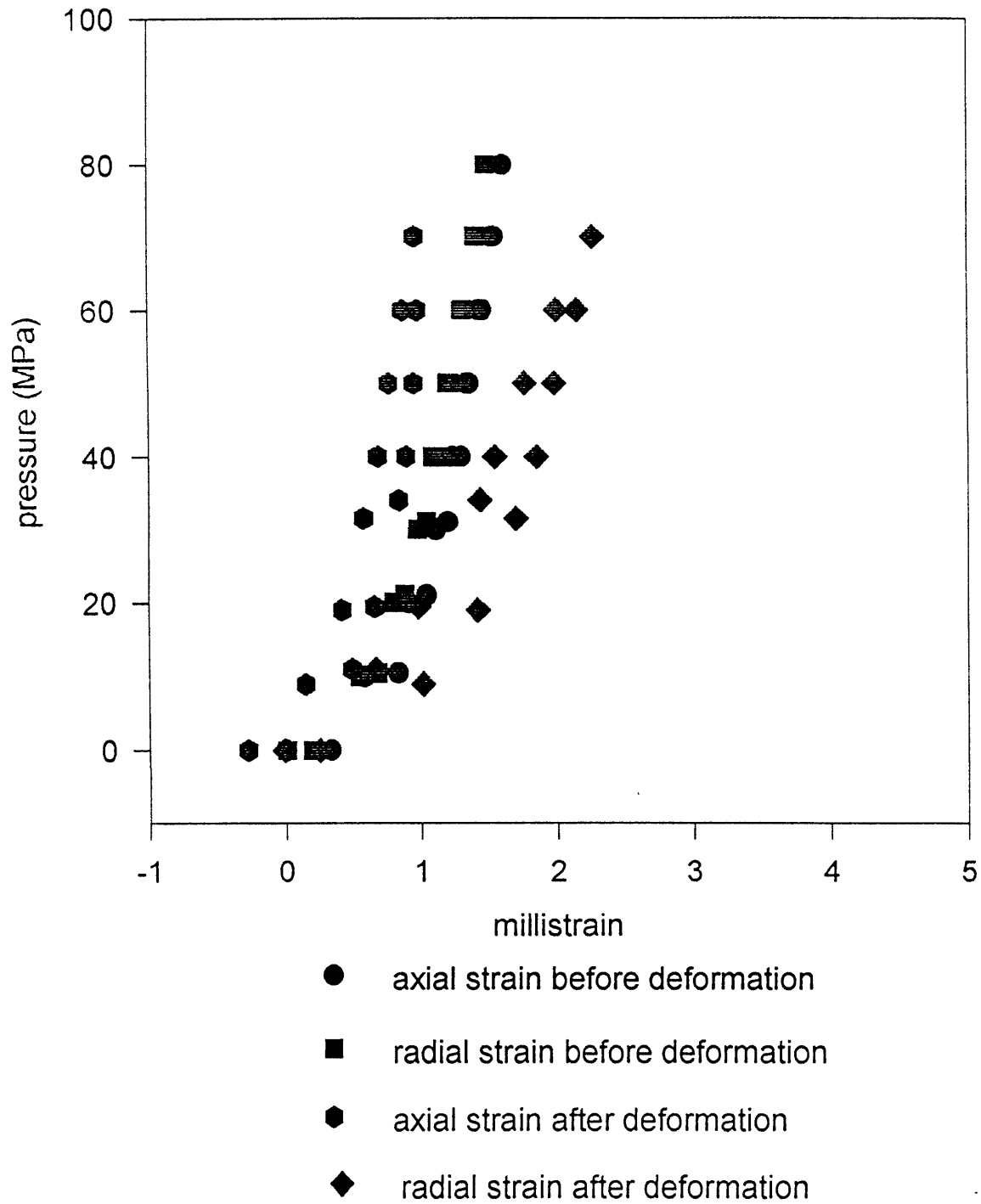
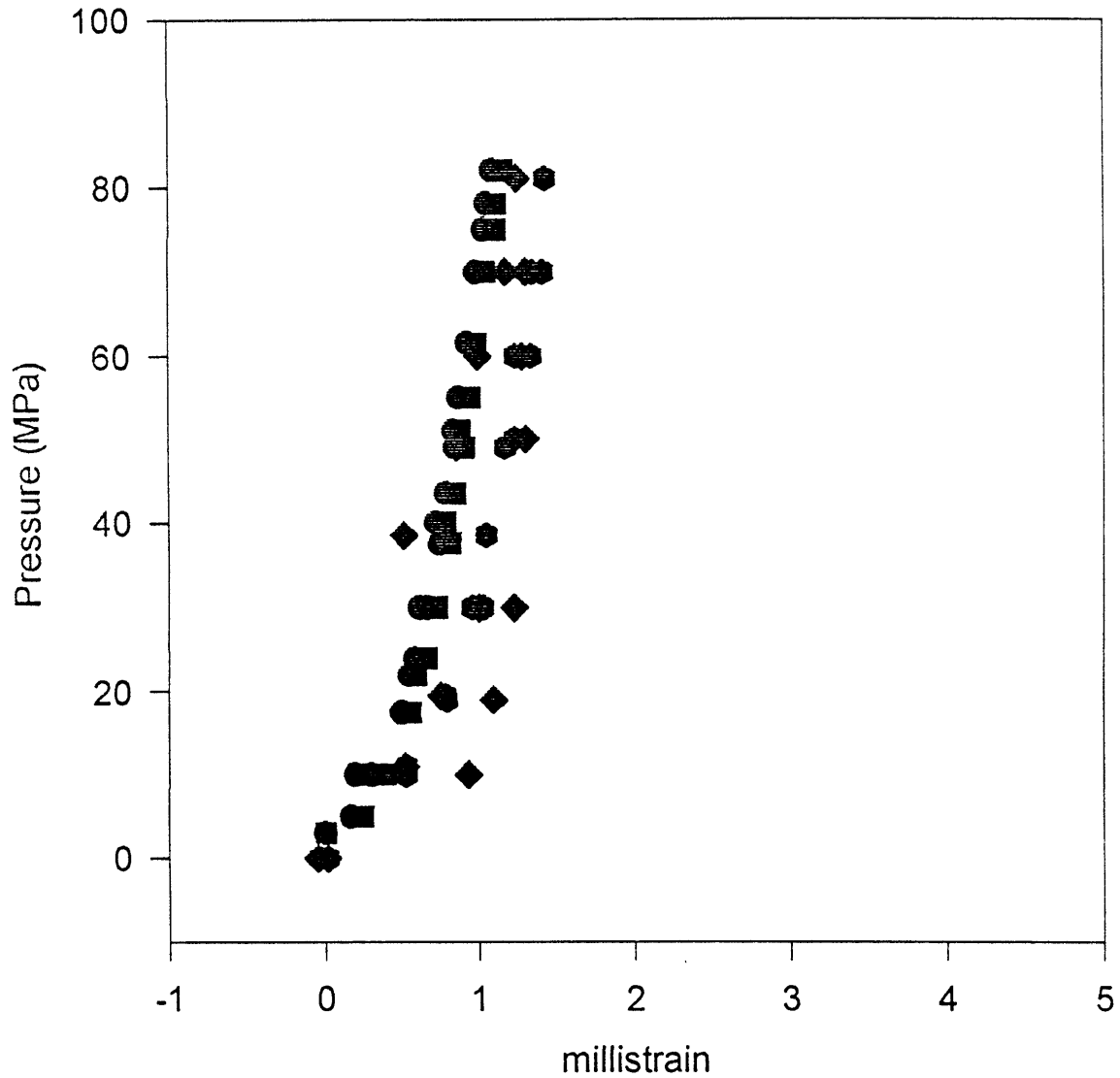
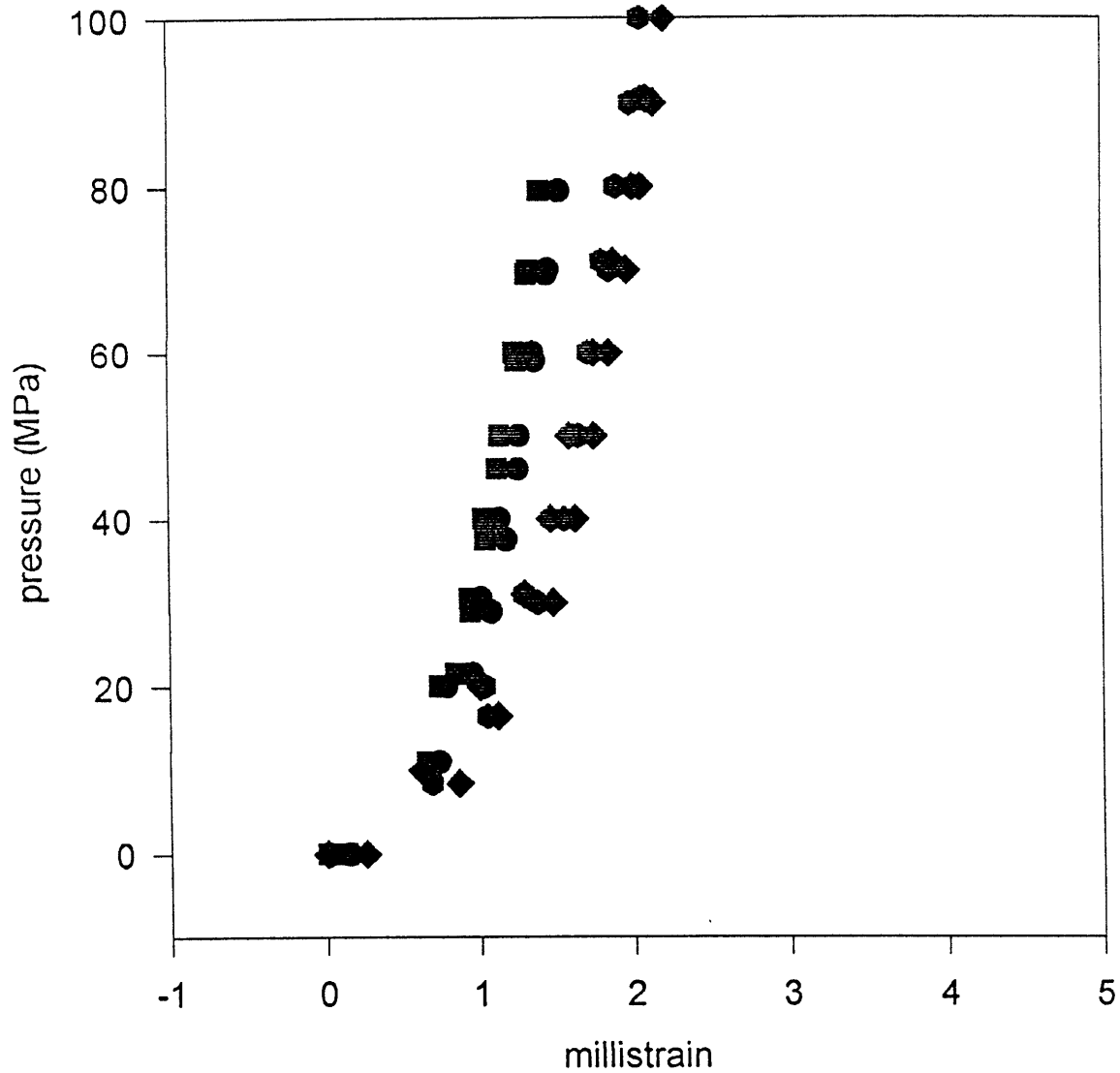
Figure 11: Linear compressibilities (3% @ 80 MPa)

Figure 12: Linear compressibilities (3% @ 100 MPa)

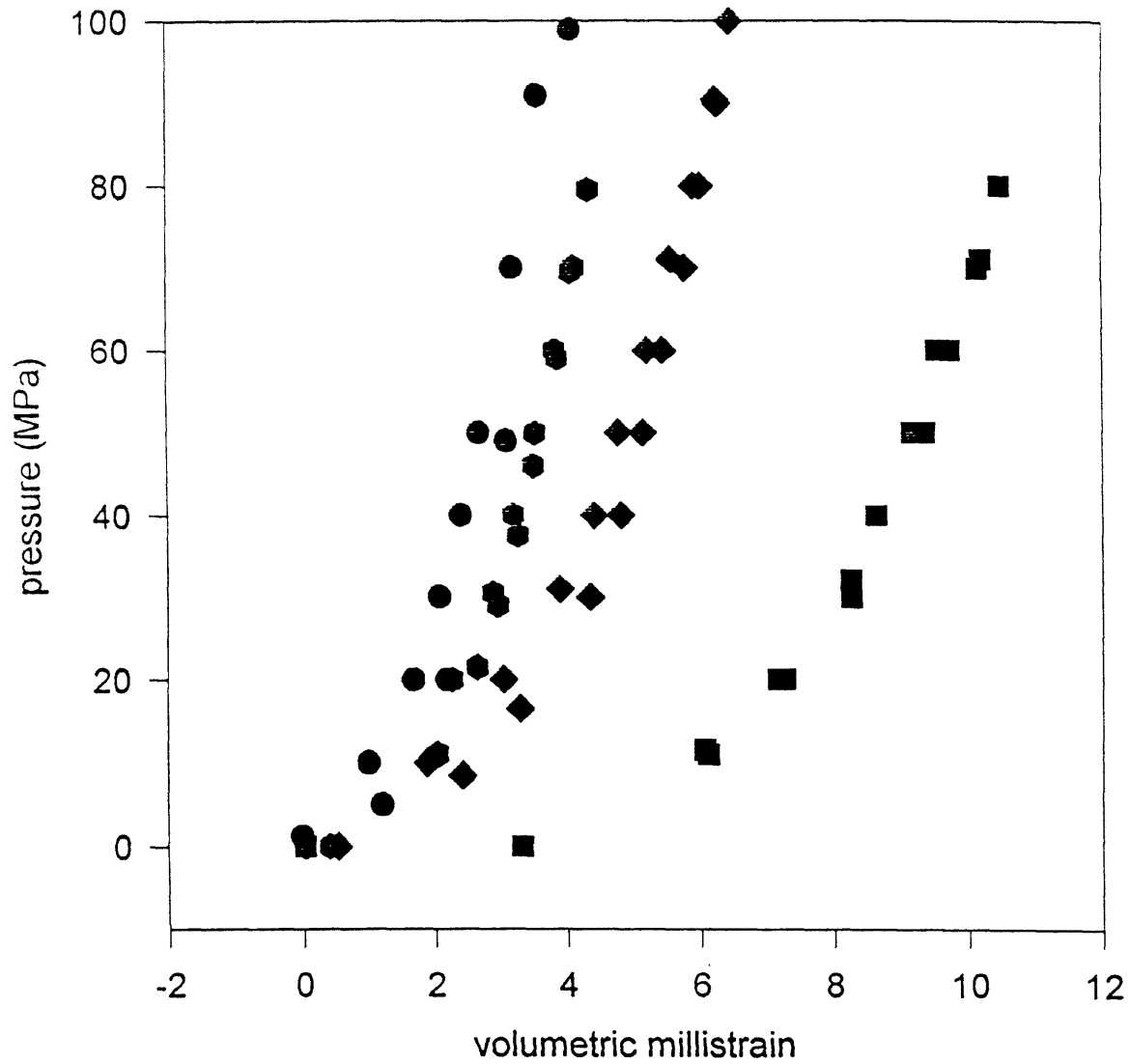
- axial strain before deformation
- radial strain before deformation
- ◆ axial strain after deformation
- ◆ radial strain after deformation

Figure 13: Linear compressibilities (3% @ 190 MPa)

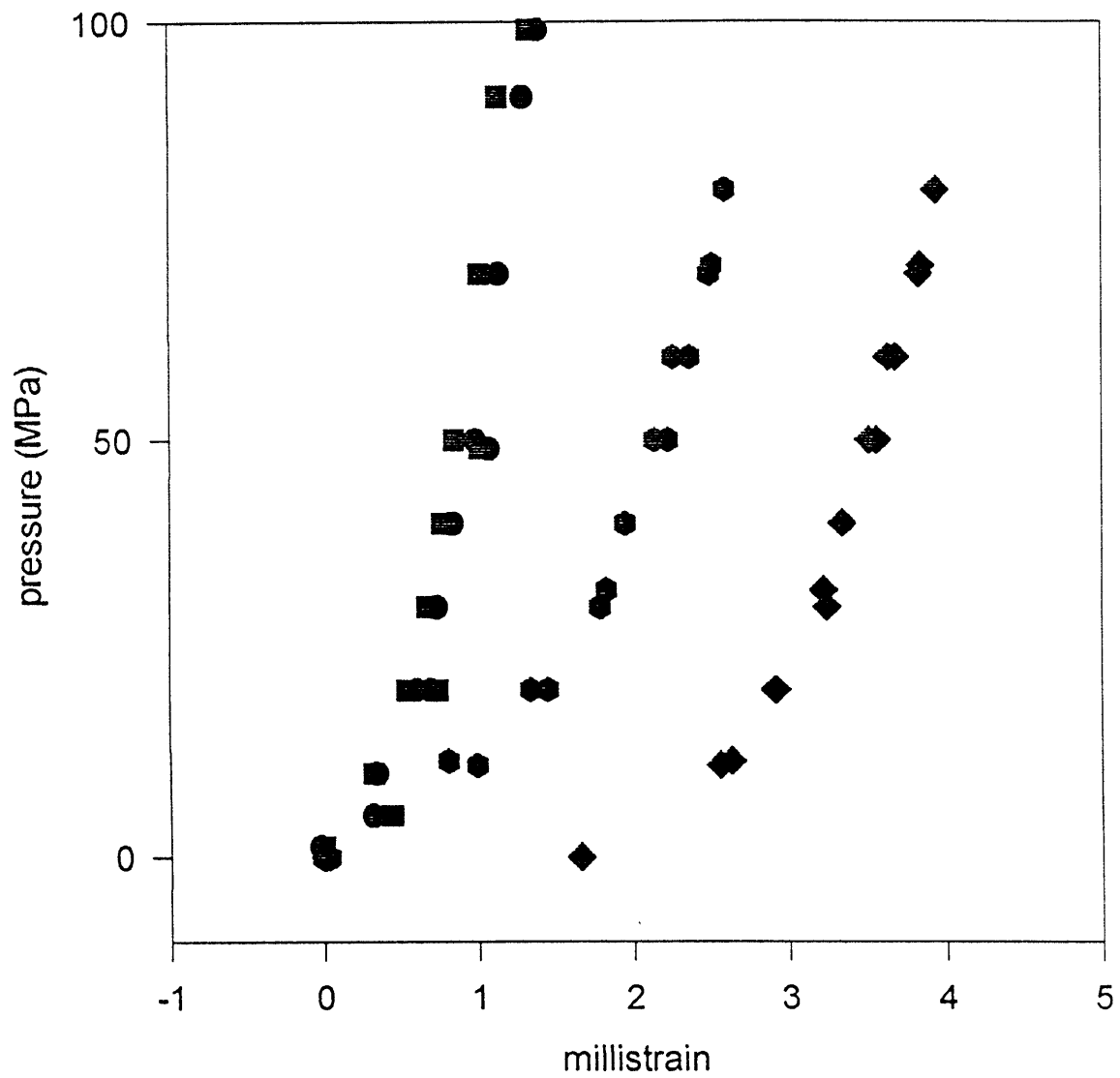
- axial strain before deformation
- radial strain before deformation
- ◆ axial strain after deformation
- ◆ radial strain after deformation

Figure 14:

Compressibilities of 3% vs. 5% ax. st.

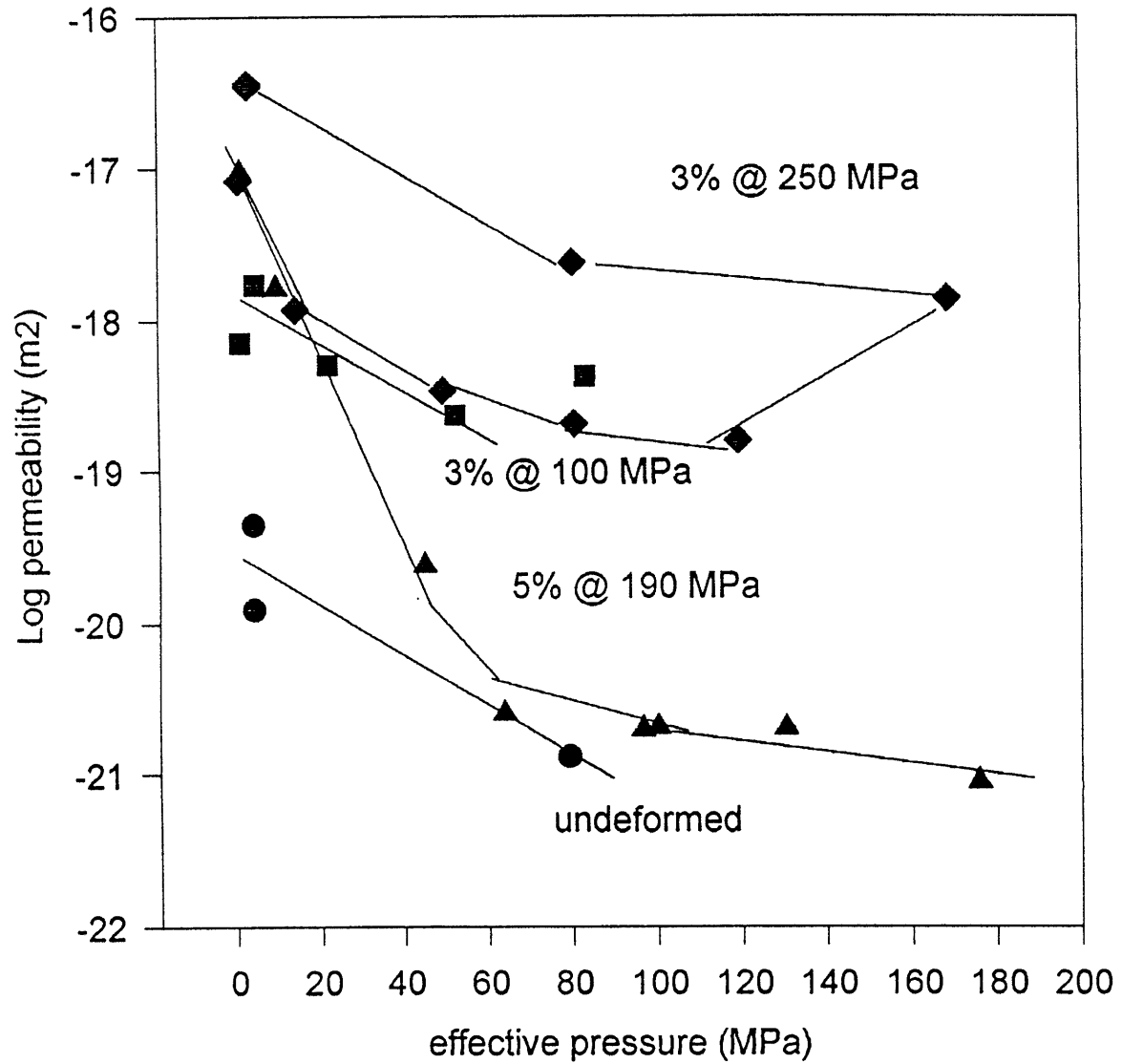


- ◆ before 3% axial strain @ 190 MPa
- ◆ after 3% axial strain @ 190 MPa
- before 5% axial strain @ 190 MPa
- after 5% axial strain @ 190 MPa

Figure 15: Linear compressibilities (5% @ 190 MPa)

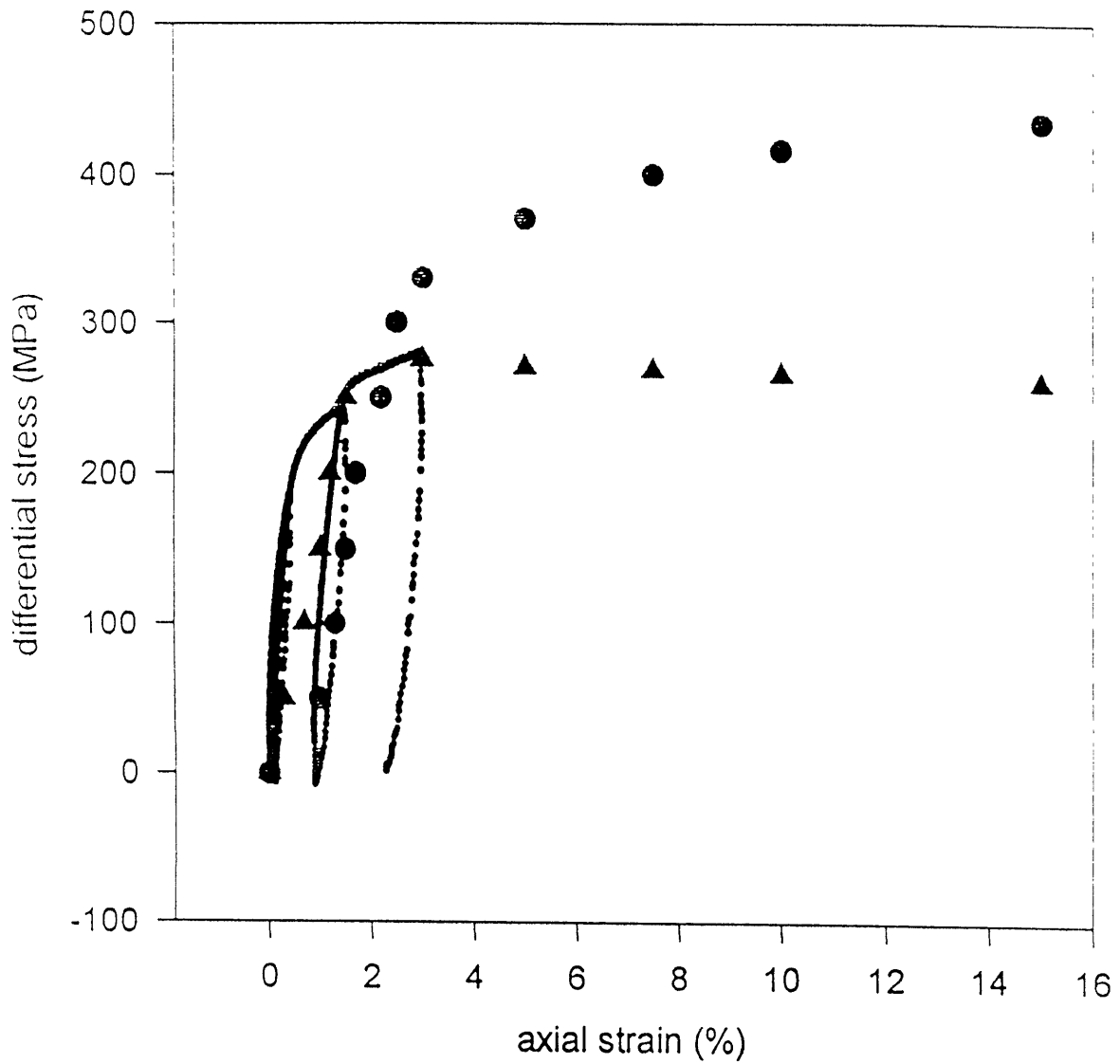
- axial strain before deformation
- radial strain before deformation
- ◆ axial strain after deformation
- ◆ radial strain after deformation

Figure 16: Log (permeability) vs. effective pressure



- undeformed
- 3% axial strain @ 100MPa
- ▲ 5% axial strain @ 190MPa
- ◆ 3% axial strain @ 250 MPa

Figure 17: Axial deformation at 100 MPa

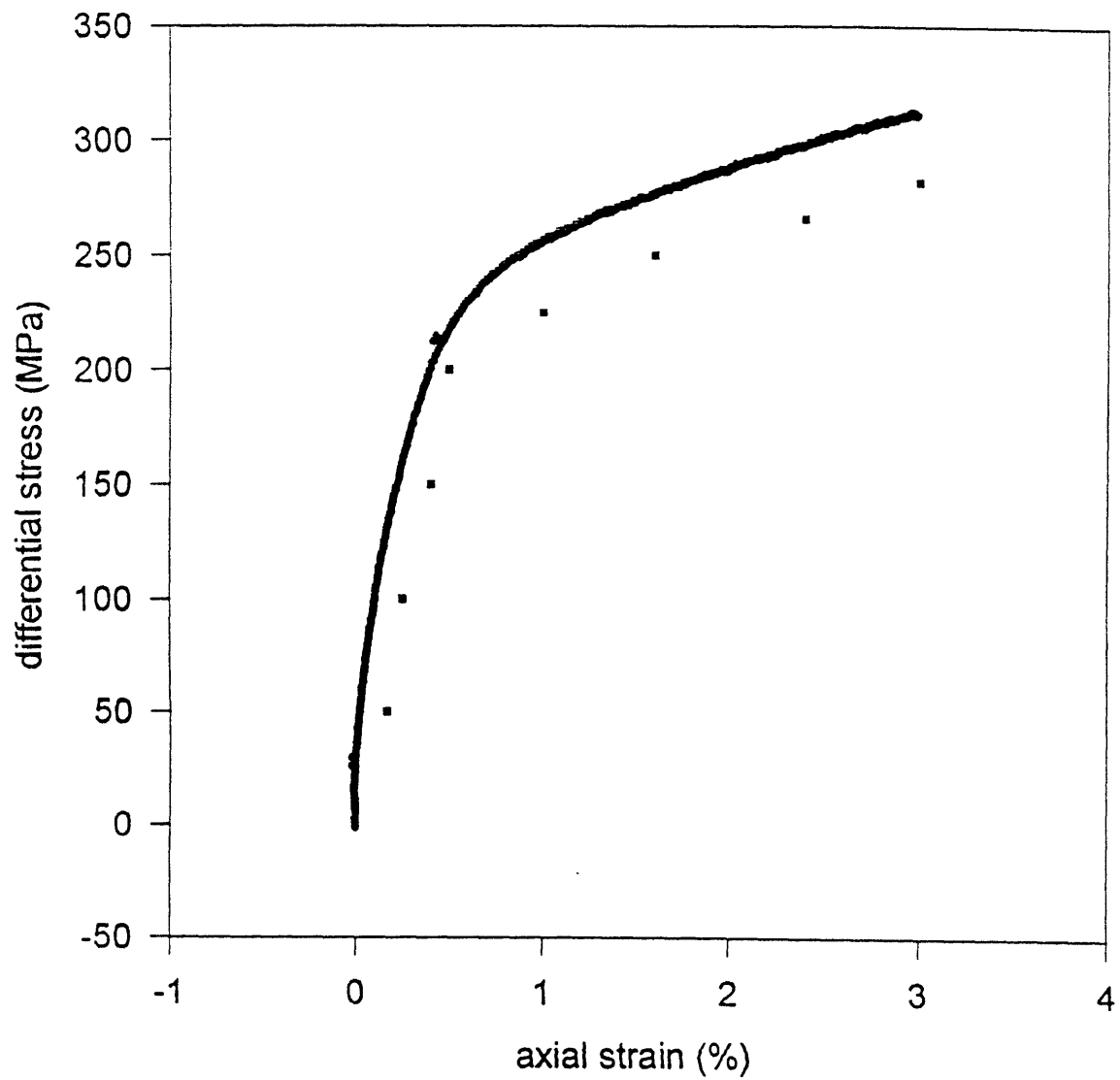


▲ Edmond (1972)

● Zhang (1994)

• this study

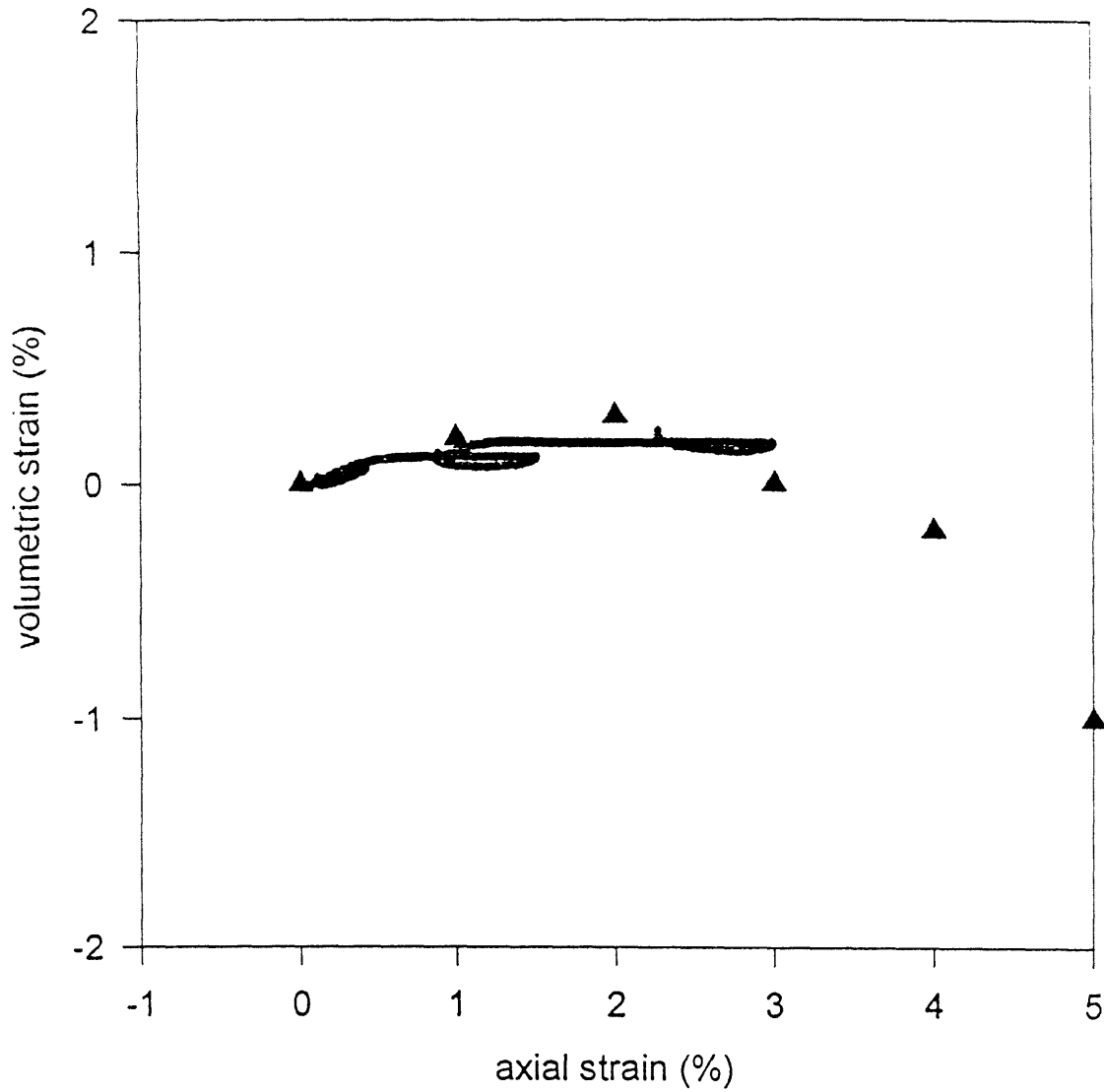
Figure 18: Axial deformation at 190 MPa



▪ Fredrich (1989)

• this study

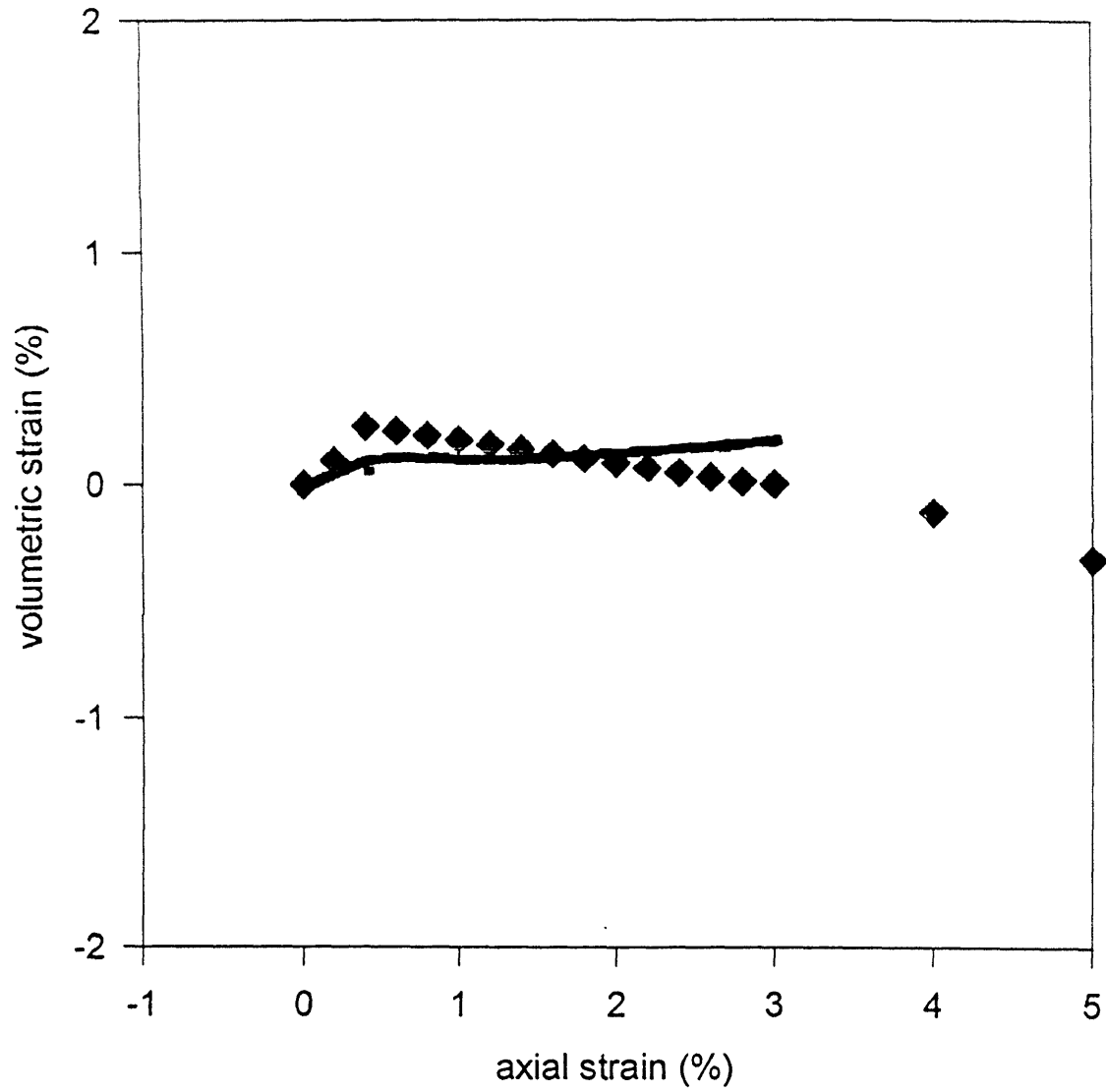
Figure 19: Volumetric strains at 100 MPa



▲ Edmond (1972)

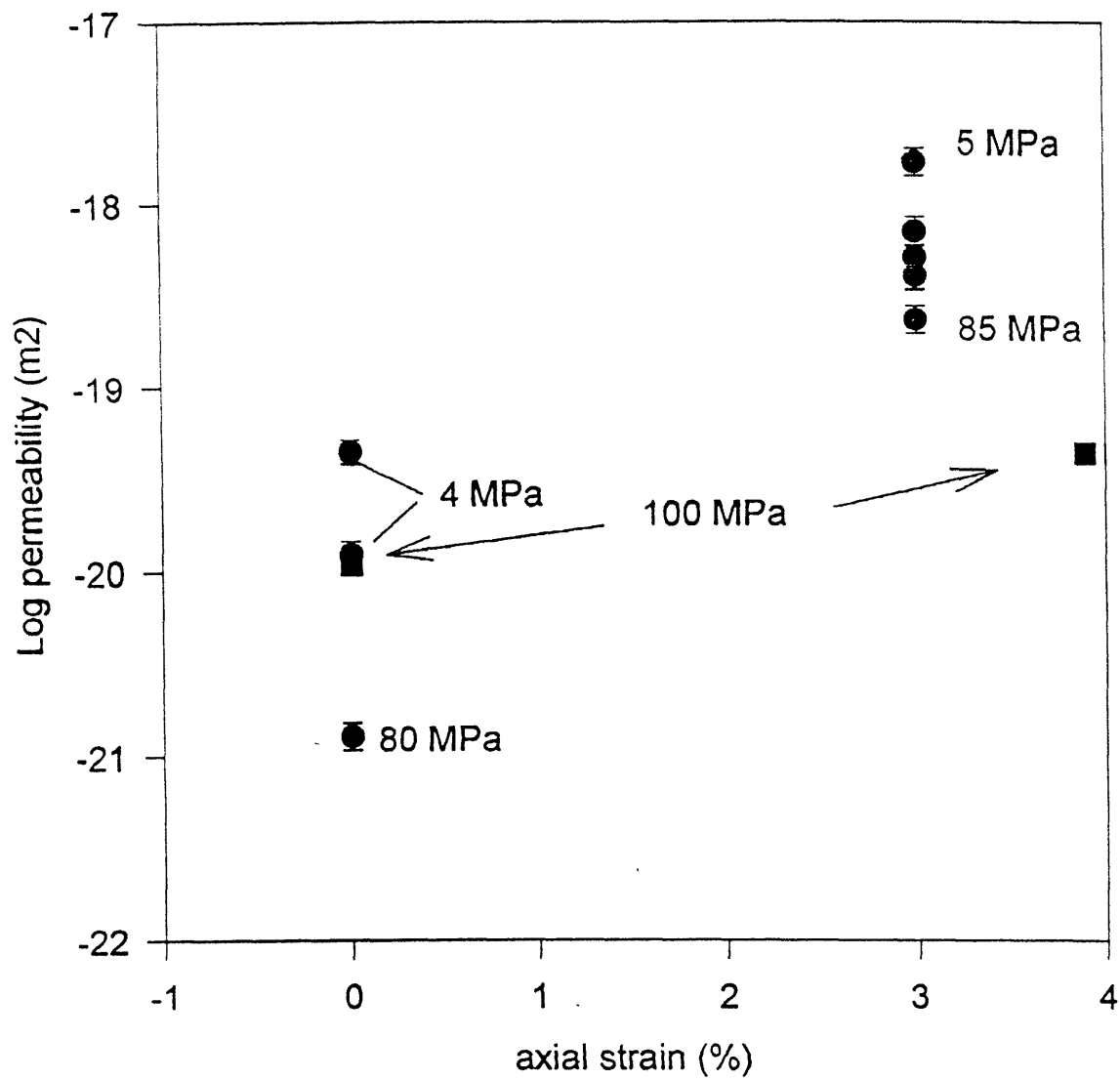
• this study

Figure 20: Volumetric strains at 190 MPa



◆ Fredrich (1989)

▪ this study

Figure 21: Permeability after deformation @ 100 MPa

■ Zhang (1994)

● this study

Table 1**Differential Stress - Axial Strain Relation**

Confining pressure (MPa)	diff. stress-ax. strain slope (MPa/ %)	linear correlation coefficient ²
250	29.27627	.928583
190	22.87178	.959025
100	16.1452	.8948734
80	11.08316	.50532

Table 2**Pressure-Volumetric Strain Relation**

Confining pressure (MPa)	Axial strain (%)	pressure-volumetric strain slope before deformation (MPa/ millistrain)	linear correlation coefficient ²	pressure-volumetric strain slope after deformation (MPa/ millistrain)	linear correlation coefficient ²	change in slope (MPa/ millistrain)
190	3	35.26542	.98457	29.89468	.951915	5.37074
100	3	39.83472	.979942	27.40948	.937693	12.42524
80	3	35.50031	.9863	20.91199	.91606	14.58832
190	5	49.87606	.989163	22.68085	.980187	27.19521

Table 3**Linear Compressibilities of 3% vs. 5% Axial Strain**

conditions	pressure/ axial strain (MPa/ millistrain)	linear correlation coefficient ²	pressure/ radial strain (MPa/ millistrain)	linear correlation coefficient ²	difference between axial and radial strain slopes
before 3% @ 190 MPa	103.1852	.979189	107.0507	.98635	-3.8655
after 3% @ 190 MPa	102.6367	.968727	83.38909	.934126	19.24761
before 5% @ 190 MPa	150.4774	.990245	148.3388	.982867	2.1386
after 5% @ 190 MPa	59.59938	.952083	65.94548	.981654	-6.3461

References

- Abdel-Gawad, M.J. Bulau, and B. Tittman, Quantitative characterization of microcracks at elevated pressure, *J. Geophys. Res.*, 92, 12,911-12,916, 1987.
- Atkinson, B.K., Subcritical crack growth in geologic materials, *J. Geophys. Res.*, 89, 4077-4114, 1984.
- Bernabe, Y., Pore volume and transport properties changes during confining pressure cycling of several crystalline rocks. *Mech. Mater.*, 5, 235-249, 1986.
- Bernabe, Y., A Wide Range Permeameter for use in rock physics. *Int. J. Rock Mech., Min., & Geomech. Abstr.*, 24, 309-315, 1987.
- Byerlee, J.D., Brittle-ductile transition in rocks, *J. Geophys. Res.*, 73, 4741-4750, 1968.
- Brace, W.F., Some new measurements of linear compressibility of rocks. *J. Geophys. Res.*, 70, 391-398, 1965.
- Brace, W.F. and E.G. Bombolakis, A note on brittle crack growth in compression. *J. Geophys. Res.*, 68, 3709-3713, 1963.
- Brace, W.F., B.W. Paulding, and C. Scholz, Dilatancy in the fracture of crystalline solids, *J. Geophys. Res.*, 71, 3939-3953, 1966.
- Brace, W.F., E. Silver, K. Hadley, and C. Goetze, Cracks and pores: a closer look, *Science*, 178, 162-164, 1972.
- Brace, W.F., J.B. Walsh and W.T. Frangos, Permeability of granite under high pressure, *J. Geophys. Res.* 73, 2225-2236, 1968.
- Edmond, J.M. and M.S. Paterson, Volume change during the deformation of rocks at high pressures, *Int. J. Rock Mech. Min. Sci.*, 9, 161-182, 1972.
- Evans, B., J.T. Fredrich, and T.F. Wong, The brittle-ductile transition in rocks: recent experimental and theoretical progress, in *The Brittle-Ductile Transition in Rocks*, edited by A. Duba, W. Durham, J. Handin, and H.F. Wang, Geophys. monogr. Ser., vol 56, pp. 1-20, AGU, Washington, D.C., 1990.
- Fisher, G.J. and M.S. Paterson, Dilatancy during rock deformation at high temperatures and pressures, *J. Geophys. Res.*, 94, 17607-17617, 1989.
- Fredrich, J.T., B. Evans, and T.F. Wong. Micromechanics of the brittle to plastic transition in Carrara Marble, *J. Geophys. Res.*, 94, 3129-4145, 1989.

- Hadley, K., Comparison of calculated and observed crack densities and seismic velocities in westerly granite, *J. Geophys. Res.*, 81, 3484-3494, 1976.
- Hirth, G. and Tullis, J., The brittle-ductile transition in experimentally deformed quartz aggregates, *J. Geophys. Res.*, 99, 11,731-11,747, 1994.
- Kachanov, M.L., A microcrack model of rock inelasticity, part I, Frictional sliding on microcracks, *Mech. Mater.* 1, 19-27, 1982.
- Kranz, R.L., Microcracking in rocks, a review, *Tectonophysics*, 100, 449-480, 1983.
- Olsen, W.A. and S.S. Peng, Microcrack nucleation in marble, *Int. J. Rock Mech. Min. Sci. Geomech. Abstr.*, 13, 53-59, 1976.
- Paterson, M.S., *Experimental Rock Deformation-the Brittle Field*, Springer-Verlag, New York, 1978.
- Rutter, E.H., On the nomenclature of mode of failure transitions in rocks, *Tectonophysics*, 122, 381-387, 1986.
- Scholz, C.H., Microfracturing and inelastic deformation of rock in compression, *J. Geophys. Res.*, 73, 1417-1432, 1968.
- Tapponnier, P., and W.F. Brace, Development of stress-induced microcracks in Westerly granite, *Int. J. Rock Mech. Min. Sci. Geomech. Abstr.*, 103-113, 1976.
- Walsh J.B. The effects of cracks on the compressibility of rock. *J. Geophys. Res.* 70, 381-389, 1965a.
- Walsh, J.B., The effect of cracks on the uniaxial elastic compression of rocks. *J. Geophys. Res.* 70, 399-411, 1965b.
- Walsh, J.B., The effect of cracks in rocks on Poisson's ratio. *J. Geophys. Res.* 70, 5249-5257, 1965c.
- Walsh J.B. and W.F. Brace, Elasticity of rock in uniaxial strain. *Int. J. Rock Mech.. Min. Sci.*, 9, 7-15, 1971.
- Walsh, J.B. and W.F. Brace, The effect of pressure on porosity and the transport properties of rock, *J. Geophys. Res.*, 89, 9425-9431, 1984.
- Willard, R.J. and J.R. McWilliams, Microstructural techniques in the study of physical properties of rocks, *Int. J. Rock Mech. Min. Sci.*, 6, 1-12, 1969.

Zhang, S. , S.F. Cox, and M.S. Paterson. The influence of room temperature deformation on porosity and permeability on calcite aggregates, *J. Geophys. Res.* 99, 15761-15775, 1994.

Zoback, M.D., and J.D. Byerlee, Permeability and effective stress, *Pet. Geol.*, 59, 154-158, 1975.